Highlights

- Nitrate removal was positively linearly related to hydraulic residence time
- Raised underdrains created immobile zones but enhanced mixing during flow events
- Dual isotopes in nitrate distinguished dentification for mobile zones for all columns
- The bottom underdrain performed best in nitrogen removal for all tested conditions
- Multiple decision criteria such as nitrate and DOC may influence underdrain height

Graphical Abstract

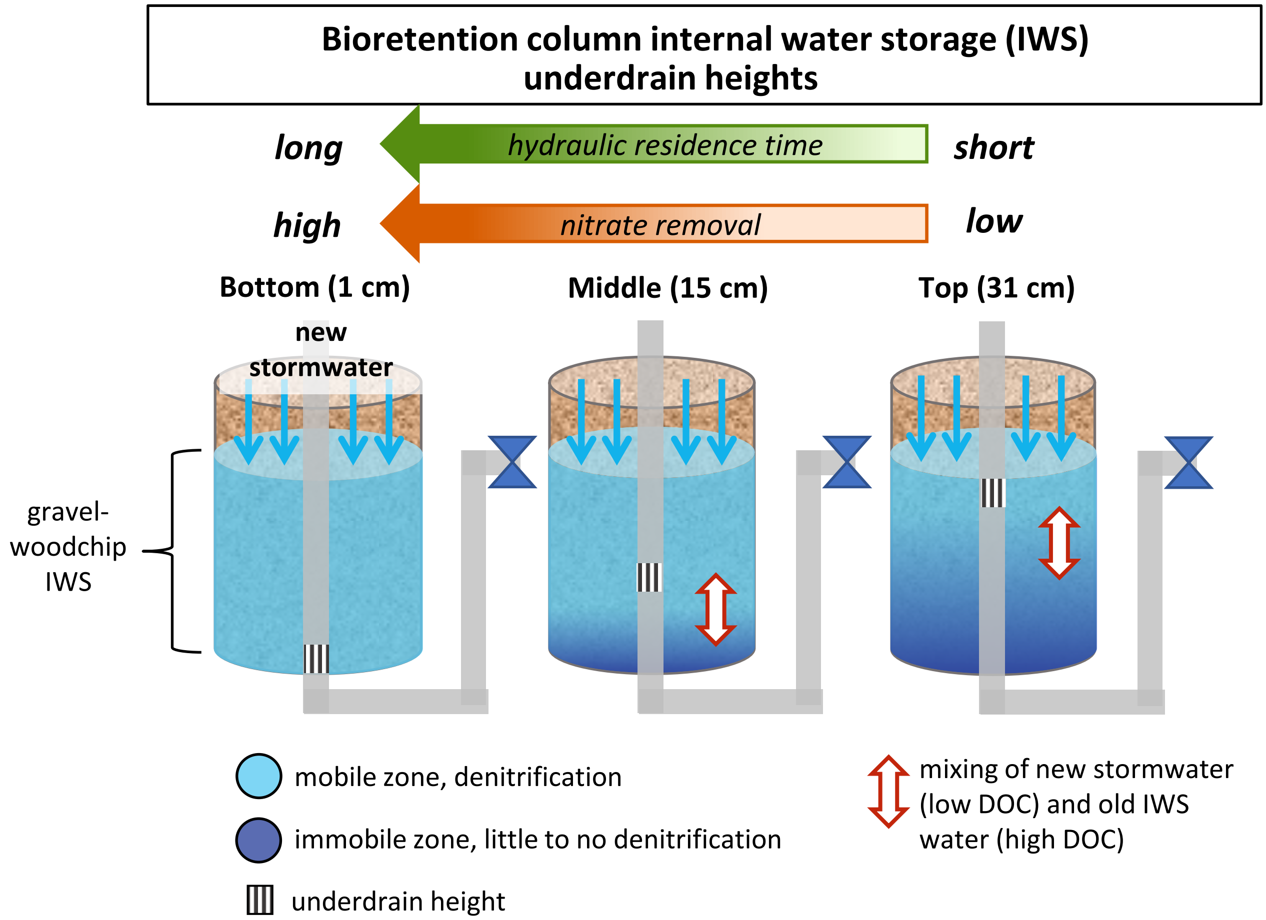

The impact of bioretention column internal water storage underdrain height on denitrification under continuous and transient flow

Adrienne G. Donaghue[a], Naomi Morgan[b], Laura Toran[b], Erica R. McKenzie[a]

[a]Department of Civil and Environmental Engineering, Temple University, Philadelphia, PA, USA

[b]Department of Earth and Environmental Science, Temple University, Philadelphia, PA, USA

Abstract

Internal water storage (IWS), a below-grade saturated layer, is a bioretention design component created by adjusting the underdrain outlet elevation. Anaerobic conditions and the presence of a carbon source in IWS facilitates denitrification. Yet it remains unclear how underdrain height within the IWS impacts nitrate (NO_3^-) removal. This study applied synthetic stormwater with NO_3^- to three laboratory columns with underdrains located at the bottom, middle, or top of a 32 cm thick gravel-woodchip IWS. Under steady state conditions, underdrain nitrogen removal demonstrated a positive linear relationship with increasing hydraulic residence time (HRT). For a 1 cm/h hydraulic loading rate (HLR), nitrogen removal efficiency increased from 52 to 99% as underdrain height moved from the top to the bottom. Despite identical IWS thickness across columns, immobilize zones below the middle and top underdrains limited the steady state nitrogen removal. Dual isotopes in NO_3^- also indicated denitrification occurred in mobile zones and showed little or no denitrification in immobile zones due to limited mass transport. Transient flow conditions were applied, to mimic storms, followed by dry conditions. Lower effluent nitrogen concentrations and mass fluxes were observed from the bottom underdrain across the range of HLRs tested (1 to 5 cm/h) but performance of all three underdrains converged after the application of one pore volume. The top underdrain enhanced mixing between new incoming low-DOC stormwater and old IWS water with high-DOC which minimized effluent DOC concentrations. NO_3^- isotope enrichment factors indicated

denitrification during transient flow for all three underdrain heights and enrichment increased for the 5 cm/h HLR. For sites with narrow IWS geometries (width to depth ratio < 1), optimal underdrain height is likely located between the bottom and top of the IWS to promote mixing with old IWS water high in DOC and sustain denitrification during storms.

Keywords:
internal water storage design, nitrogen management, dual nitrate isotopes, urban stormwater quality, DOC, immobile zones

1. Introduction

Urban runoff is considered a major pollutant source to receiving waters. Nutrients, such as nitrogen, conveyed in runoff cause habitat degradation and algal blooms which are expected to worsen with population growth and climate change (Whitehead et al., 2009). Green stormwater infrastructure (GSI) is implemented in urban landscapes to protect water resources. Bioretention is a passive GSI strategy that employs multiple functions (ponding, infiltration, biotic processes, and water storage) to manage runoff quantity and water quality. The main design components include a vegetated basin filled with engineered media. An underdrain is often incorporated in a gravel layer below engineered fill media to collect a portion of infiltrated stormwater and discharge to the sewer network or receiving waterbody.

Internal water storage (IWS) is a subsurface bioretention design component created by raising the outlet elevation of the underdrain. For combined sewer systems, IWS provides additional storage volume and water is primarily released via exfiltration into native media. For separate sewer systems, sites with less permeable soils, or nutrient sensitive watersheds, IWS can be implemented for water quality improvements (Brown et al., 2009). Nitrate (NO_3^-) removal in bioretention occurs via plant uptake or biotic processes including denitrification or dissimilatory NO_3^- reduction to ammonia (DNRA) (Bu et al., 2017; Igielski et al., 2019; Li et al., 2019). When the IWS remains saturated and a carbon source is available (often leached from woodchips), IWS provides favorable conditions for denitrification and NO_3^- is reduced to nitrogen gas (N_2)(Kim et al., 2003). IWS design often connects the perforated underdrain, located at the base of the gravel layer, to an upturned elbow. Alternatively, a raised underdrain can be positioned at the top of the IWS to achieve the same thickness and storage capacity (Donaghue et al., 2022). However, the impact of IWS underdrain configuration on NO_3^- removal needs to be evaluated.

Understanding the impact of IWS design choices on water quality, specifically NO_3^-, advances design and informs practitioners. Increased hydraulic residence time (HRT) corresponds to increased NO_3^- removal (Halaburka et al., 2017; Igielski et al., 2019). For example, one study demonstrated that HRT accounted for 93% of NO_3^- removal compared to the variables of dissolved oxygen (DO), temperature, and influent NO_3^- concentration (Martin et al., 2019). We previously employed bioretention columns and modeling to demonstrate that raised underdrain heights, with respect to the bottom of the IWS, introduced nonideal flow regions, or immobile zones. Raised underdrain heights reduced hydraulic efficiency and consequently the measured HRT (Donaghue et al., 2022). It is expected that IWS underdrain height would influence NO_3^- removal efficiency which served as a primary motivation to this study. In urban environments, space limitations and property costs present challenges for GSI implementation. Understanding the impact of IWS underdrain height on NO_3^- removal, particularly in narrow systems, can allow design flexibility without compromising water quality goals.

Because IWS underdrain height induces different flow patterns, the consideration of how IWS underdrain height impacts NO_3^- dynamics as a function of rain intensity and dry periods is critical. Under intense precipitation, faster infiltration rates into the IWS can shorten HRTs and consequently reduce NO_3^- removal. Optimizing IWS underdrain configuration to site specific characteristics could combat these effects and maximize NO_3^- removal during precipitation. During antecedent dry periods (ADP), woodchips leach dissolved organic carbon (DOC) into IWS porewater and DOC concentrations can increase as ADP increases (Lynn et al., 2015a). However, during prolonged ADPs evapotranspiration and exfiltration to underlying media can expose woodchips at the top of the IWS to unsaturated conditions. Others have shown that woodchips in unsaturated layers degrade faster than saturated woodchips and can export higher DOC and organic nitrogen (Lynn et al., 2015a). The selection of an appropriate IWS underdrain configuration may require balancing multiple water quality parameters such as NO_3^- and DOC.

Dual isotopes in NO_3^- is a tool gaining traction to characterize nitrogen processing in stormwater (Burgis et al., 2020; Burns et al., 2009; Carey et al., 2013; Yang and Toor, 2016). Dual isotopes refer to the analysis of both the nitrogen isotopes (^{14}N and ^{15}N) and the oxygen isotopes (^{16}O and ^{18}O) in NO_3^-. Isotopes can be useful for identifying transformation processes when the process preferentially favors an isotope, leading to fractionation. For example, a kinetic isotope effect is created during microbial denitrification, as organisms preferentially consume lighter nitrogen and oxygen isotopes (^{14}N and ^{16}O); this depletion creates solute NO_3^- enriched in heavier isotopes (^{15}N and ^{18}O)(Mariotti et al., 1981; Zhang et al., 2019). Consequently, denitrification is marked by a predominantly linear, positive trend in both the $\delta^{15}N$ and $\delta^{18}O$. Batch experiments demonstrated microbial denitrification can cause isotopic fractionation within tens of minutes to several hours (Currie, 2007; Kim et al., 2003; Sebilo et al., 2019). However, isotope patterns in flow-through systems such as IWS are not well-studied. Here, column experiments coupled with dual isotope analysis contribute to understanding the application of nitrogen isotopes in GSI systems.

This work employs three laboratory bioretention columns comprised of a gravel-woodchip IWS with varying underdrain height to distinguish microbial denitrification from dilution under steady state and transient flow. Steady state conditions considered the effect of HRT on NO_3^- removal efficiency and NO_3^- removal kinetics. Transient conditions evaluated the effect of hydraulic loading rate (HLR) and ADP on IWS water quality, NO_x dynamics, and potential denitrification during flow events.

2. Materials and methods

2.1. Bioretention column design

IWS underdrain height varied across three cylindrical bioretention columns (28.8 cm ID × 82 cm height) (Fig. 1a) by adjusting the elevation of 2 cm thick screened openings on the center PVC pipe as follows: 0 to 2 cm bottom column (1 cm, Fig. 1b), 14 to 16 cm middle column (15 cm, Fig 1c), and 30 to 32 cm top column (31 cm, Fig. 1d). IWS media included a blend of pea-gravel and hardwood woodchips at a ratio of 2:1 by volume; the mixture and ratio were selected based on performance reported by others (Lynn et al. 2015b). Further details regarding column media are provided in the SI and our previous work (Donaghue et al., 2022). The center PVC pipe connected to an upturned elbow outside each column. The invert elevation of the outlet was 30 cm above the column base to maintain a constant IWS thickness across all columns. The IWS included two sample port groups located 5 cm (proximal, P) and 10 cm (distal, D) from the center PVC pipe, respectively. The sample port heights were 5, 10, 20, and 25 cm above the column base (Fig. 1a). Sample identification notes the sample group followed by sample height. For example, P-20 refers to the proximal IWS sample port 20 cm above the column base. Sampling also included the underdrain effluent.

Figure_1

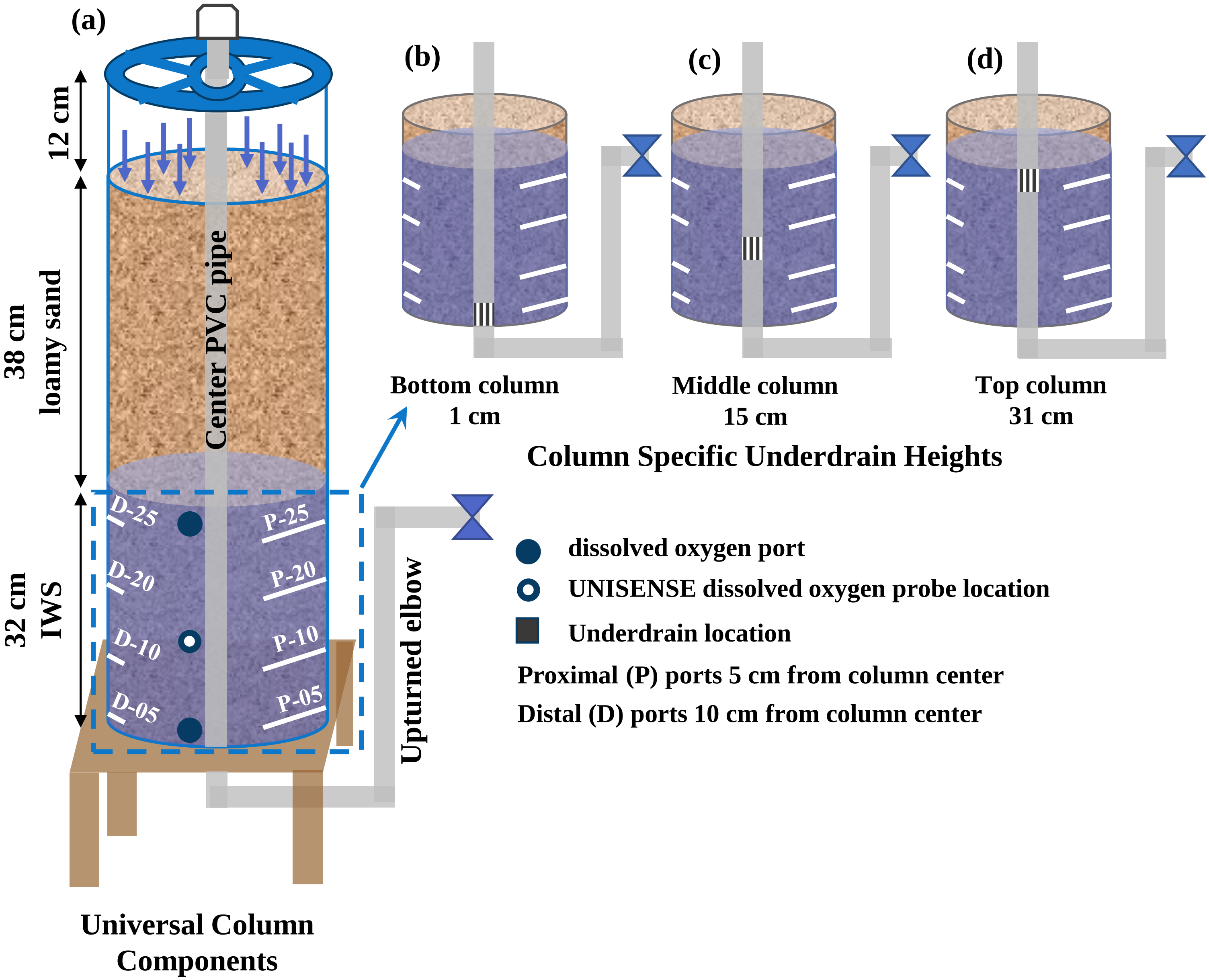

Fig 1
Universal column schematic (a) and underdrain configurations for the bottom (1 cm) (b), middle (15 cm) (c), and top (31 cm) (d) underdrain heights. The IWS was comprised of pea gravel and hardwood woodchip at a 2:1 ratio by volume.

2.2. Key nomenclature

Bioretention columns were differentiated by the height of the underdrain using the terms: bottom column (1 cm), middle column (15 cm), and top column (31 cm). When referring to the underdrain sample location we used the terms bottom, middle, or top underdrain. Our previous study (Donaghue et al., 2022) employed tracer studies and USGS VS2DRTI (USGS, 2019) modeling to characterize IWS hydraulics. Results demonstrated the presence of mobile zones (areas of flowing water) generally above the underdrain and immobile zones (low flow or stagnant areas) below the middle and top underdrain. To account for the presence of immobile zones, measured HRT was calculated by multiplying the volume of column media by the effective pore volume (PV; which considers only the mobile region) divided by flow rate (Equation S1).

The experimental design included steady state ("SS"; continuous flow) and transient ("Trans"; intermittent flow) events. Replicate transient events were conducted for each condition and are indicated using capitol roman numerals. Flow conditions were conducted at HLRs of 1, 2.5, and 5 cm/h, which was also included in the event name. Transient events considered three different ADPs (2.8, 6.8, and 13.8 days) defined here as the dry time between the end of the transient event (x) and the start of event (x+1). For reporting purposes, nominal ADPs are used (i.e., 3, 7, and 14 days). The term "old" IWS water describes water stored in the IWS between transient events and "new" water refers to fresh incoming synthetic stormwater applied to the top of the column (Wang et al., 2018). The final event concentration refers to the final sample collected at t=300 minutes during transient events. While NO_3^- was the only nitrogen source added to synthetic stormwater, column samples were analyzed for total nitrogen (TN), total dissolved nitrogen (TDN), ammonium/ammonia (NH_4^+/NH_3), and NO_x (the sum of NO_3^- plus nitrite (NO_2^-)). Nitrite comprised less than 5% of NO_x (monitored during events SS-5 and SS-2.5); therefore, analysis was limited to NO_x for events following and was assumed to be predominantly NO_3^-. NO_x and DOC mass loads released from the underdrain during flow were used to assess column performance. Mass loads were determined by integrating the area under the underdrain concentration curve using the trapezoidal method. Mass flux (mg/m^2 for a given transient even) equals the total mass load released from the underdrain during flow divided by the column horizontal cross-sectional area (0.064 m^2).

2.3. Synthetic stormwater preparation and application

Synthetic stormwater was prepared using deionized water or reverse osmosis water in a 246 L tank. NO_3^-, in the form of sodium nitrate, was added at a nominal concentration of 3 mg-N/L which agreed with other column studies (Igielski et al., 2019; Kim et al., 2003; Peterson et al., 2015) and mimics NO_3^- porewater concentrations observed for monitored field sites in Philadelphia, PA. Synthetic stormwater also included: orthophosphate (0.1 mg-P/L) to support microbial growth, sodium chloride (58.4 mg/L) for ionic strength, and sodium bicarbonate (252 mg/L) for buffering capacity (Table S1). The pH was adjusted to ~7.0 using hydrochloric acid. Synthetic stormwater was applied to the top of columns using a Masterflex L/S digital drive peristatic pump (Cole-Parmer) and evenly distributed through a polyethylene ring with equidistant perforations.

2.4. Water quality analysis

For steady state water quality parameters measured included pH, DOC, NH_4^+/NH_3, NO_x, DON, PON and TN from the underdrain and NO_x from IWS sample ports (Table S3). DO was measured in the IWS using a UNISENSE Oxygen MiniOptode 3000 µm (UniSense, Denmark). UNISENSE probes were located at 15 cm above the column base. Underdrain flow rates were measured gravimetrically by collecting underdrain effluent for one minute in a beaker. The mass was then measured and converted to mL/min. DOC and pH were measured for the underdrain location only. For steady state, DOC was determined by catalyzed combustion using a TOC-V CHS Analyzer (Shimadzu). DOC samples from SS-1HLR exceeded holding times following COVID lab restrictions and were not analyzed. For transient events, UV absorbance (254 nm) was measured using an Agilent 8453 spectrophotometer and was employed as a surrogate for DOC (e.g., similar to Abusallout and Hua, 2017; Berger et al., 2019). Samples were analyzed the same day of collection. pH was measured using a Thermo Scientific Orion Versa Star module.

Nitrogen chemistry analysis included TN, TDN, NO_x, and NH_4^+/NH_3 using an AQ300 Discrete Analyzer (SEAL Analytical). Samples for dissolved constituents were centrifuged at 1,000 x g for 8 min to remove particulates and bacteria. NO_x and NH_4^+/NH_3 were analyzed in accordance with EPA methods 126-D Rev. 0 and 150-A Rev. 2, respectively. TN (uncentrifuged) and TDN determination used peroxodisulfate oxidation digestion (Ebina et al., 1983) followed by NO_x analysis described above. Particulate organic nitrogen (PON=TN-TDN) and dissolved organic nitrogen (DON=TDN-NO_x-NH_4^+/NH_3) were determined by difference. AQ300 batch analysis included continued calibration verification (CCV), continued calibration blank (CCB), and reference material (Hach 2833249) quality control samples analyzed every 10 samples. For digested TN and TDN samples, an ammonium reference material (2.5 mg-N/L) was included with each batch as a quality control measure for digestion recovery (conversion of NH_4^+ to NO_3^-). Acceptance criteria for quality control samples and the digested reference material sample was ±10% of the known concentration. Error propagation for DON concentrations determined by difference was calculated using the standard deviation of replicates for NO_x and NH_4^+/NH_3 chemistries reported in method precision studies. When considering the 2.5 mg-N/L digested reference material, this corresponded to an uncertainty less than 5%. Sample preservation and analytical detection limits are reported in Table S6.

2.5. Isotopic analysis and enrichment factor calculations

Stable isotope samples for NO_3^- were collected at the end of each steady state event from the underdrain location and sample ports D-10 and D-25 (Table S3) and during transient events (Table S4). Isotope samples were filtered (0.45-µm) and stored frozen in 30-mL wide-mouth high-density polyethylene (HDPE) bottles (Thermo Scientific™, DWK Life Sciences Wheaton™ Leak-Resistant). Isotope analysis was conducted at the Davis Stable Isotope Facility (SIF), University of California. Samples selected for ^{15}N and ^{18}O analysis had NO_x measurements above SIF lower limit of quantitation (0.4 µM or ~0.05 mg-N/L) and methods followed a bacteria denitrification assay (University of California Davis Stable Isotope Facility, 2021). Nitrogen (N) and oxygen (O) content in column samples were compared to laboratory reference materials with known ^{15}N and ^{18}O. Analytical results were presented in delta notation (δ), expressed as parts per mil (‰), based on the following formulas:

$$\delta^{15}N = [(^{15}N/^{14}N)_{sample}/(^{15}N/^{14}N)_{reference\ material}\ x\ 1000] \qquad (1)$$

$$\delta^{18}O = [(^{18}O/^{16}O)_{sample}/(^{18}O/^{16}O)_{reference\ material}\ x\ 1000] \qquad (2)$$

The presence of denitrification is suggested when decreasing NO_x concentrations coincided with increasing $\delta^{15}N$-NO_3^- and $\delta^{18}O$-NO_3^- along a linear slope between 0.5 and 1.0 (Kendall et al., 2007). When isotopic signatures suggested denitrification, enrichment factors (ε) provided an estimation of column denitrification efficiency. Enrichment factors were calculated using the isotopic ratios in equations 3 and 4:

$$\varepsilon_{15N} = (\delta\ 15N_{sample} - \delta\ 15N_{initial})/ln(NO_3^-{}_{sample}/NO_3^-{}_{initial}) \qquad (3)$$

$$\varepsilon_{18O} = (\delta\ 18O_{sample} - \delta\ 18O_{initial})/ln(NO_3^-{}_{sample}/NO_3^-{}_{initial}) \qquad (4)$$

where difference between sampled and initial isotope values are compared to the fraction of NO_3^- concentration remaining. The enrichment factor is the slope of the linear trend between the isotope difference and concentrations on a log normal scale and more negative ε indicates more efficient microbial denitrification. Enrichment factors were determined for ^{15}N-NO_3^- and ^{18}O-NO_3^- for select steady state and transient events. It was assumed NO_x equaled NO_3^- for enrichment factor calculations.

2.6. Steady state events

Steady state (SS) considered the three events SS-5HLR, SS-2.5HLR, and SS-1HLR (Table 1; additional detail in Table S2) which corresponded to HLRs of 5, 2.5, and 1 cm/h, respectively. Before initiating SS, tracer studies described elsewhere occurred under continuous flow from November 2019 to January 2020; approximately 32 total PVs were applied to each column during this time (Donaghue et al., 2022). The IWS remained fully saturated during SS-5 through SS-1 (February 2020 to March 2020). For each event, flow application remained constant until the relative standard deviation of NO_x concentrations varied less than 30% for three consecutive measurements at the underdrain and mobile zone IWS sample ports. This generally occurred within 5 days. The average influent synthetic stormwater NO_3^- concentration for steady state was 2.90 ± 0.26 mg-N/L. Samples were generally collected daily Monday through Friday and analyzed for parameters listed in Table S3.

The steady state NO_x removal efficiency was determined at the underdrain location using equation 5

$$NO_x\ (\%) = \left(\frac{C_{influent} - C_{underdrain}}{C_{influent}}\right) * 100 \qquad (5)$$

Table 1. Column event sequence.

Event	HLR	Bottom U. (0 cm)		Middle U. (15 cm)		Top U. (30 cm)		ADP[d]
		Flow	*HRT*	*Flow*	*HRT*	*Flow*	*HRT*	
	cm/h	*avg. mL/min*	*Eff PV[c] h*	*avg. mL/min*	*Eff PV[c] h*	*avg. mL/min*	*Eff PV[c] h*	*days*
SS-5HLR	5	50.2	4.7	53.0	3.7	51.9	2.8	--
SS-2.5HLR	2.5	26.1	9.4	26.2	7.4	26.4	5.6	--
SS-1HLR	1	10.7	21.9	11.2	17.4	11.4	13.2	--
Dormant Period[b] (3/16/2020 - 8/10/2020)								
SS-1.5HLR-post-dormant		13.8	17.6	13.6	13.9	14.0	10.5	--
Trans-1HLR-I	1	11.8	--	11.0	--	11.3	--	6.8
Trans-1HLR-II	1	10.9	--	10.6	--	10.6	--	6.8
Trans-2.5HLR-I	2.5	*Not sampled*						6.8
Trans-2.5HLR-II[e]	2.5	28.0	--	27.2	--	26.7	--	6.8
Trans-2.5HLR-III[e]	2.5	25.6	--	26.5	--	26.2	--	6.8
Trans-5HLR-I	5	*Not sampled*						6.8
Trans-5HLR-II	5	54.3	--	55.1	--	55.3	--	6.8
Trans-5HLR-III	5	53.1	--	51.5	--	53.7	--	6.8
Trans-14ADP-I	2.5	25.3	--	25.9	--	24.9	--	13.8
Trans-3ADP-I	2.5	25.1	--	26.1	--	25.6	--	2.8
Trans-14ADP-II	2.5	26.6	--	25.9	--	26.1	--	13.8
Trans-3ADP-II	2.5	27.1	--	26.8	--	27.7	--	2.8

A detailed version of this table in included in the Supplementary Data

[a] steady state (SS) flow refers to continuous flow conditions. Transient flow events were applied for a 5 h duration

[b] During COVID, lab access was restricted and columns experienced a dormant period from March 2020 to August 2020.

[c] hydraulic residence time (HRT) was calculated based on effective pore volume (PV); in other words, the portion of pore volume that contributed to flow.

[d] Antecedent dry period (ADP) equals the number of days between events; nominal ADP reported in the event name.

[e] Events Trans-2.5HLR-II and Trans-2.5HLR-III also correspond to Trans-7ADP scenarios.

where $C_{influent}$ equals the synthetic stormwater NO_x concentration (~3 mg-N/L) and $C_{underdrain}$ equals the observed underdrain effluent NO_x concentration. Significant differences across steady state events were determined using a paired t-test (α of 0.05).

SS-1HLR finished on March 16, 2020 after 5 months of continuous operation. Due to interruptions in lab access associated with COVID restrictions, the columns sat dormant for 4.5 months (March through August 2020) and a portion of the IWS became unsaturated during the dormant period. Upon returning to the lab, a pulse tracer test was performed for all columns to establish a new baseline for hydraulics (see SI for details). SS-1.5-postdormant was introduced at a HLR of ~1.5 cm/h to reacclimate denitrifying conditions before transitioning to transient flow events. During SS-5HLR through SS-1.5-postdormant ~110 total PVs were applied to each column.

2.7. Transient events

Transient flow provided an environmentally relevant representation of episodic storm and dry conditions. Transient events lasted five hours (300 min) and considered HLRs of 1, 2.5, and 5 cm/h and ADPs of 3, 7, and 14 days. Table 1 reports transient event sequencing; the event identification notes either the HLR or ADP testing scenario and the event replicate (i.e., I, II, or III). For example, Trans-2.5HLR-II refers to transient flow at a 2.5 cm/h HLR, replicate two. For ADP transient events, a HLR of 2.5 cm/h was applied. After event Trans-2.5HLR-I, different initial IWS water levels were observed. Each IWS was upfilled using reverse osmosis water prior to the start of the event to ensure IWS water level depths were consistent across columns (low NO_3^-~0.4 mg-N/L, and phosphorous, ~0.2 mg-P/L, concentrations). Reverse osmosis water was applied through the center PVC pipe (filling the IWS from the screened opening upward) and pumped at a flow rate of 20 mL/min. This approach was adopted for the remainder of transient events.

Transient sampling followed the frequency listed in Table S4. Samples were collected immediately before flow application (t = 0 min) and then at time points of 100, 140, 180, 220, 260, 300 min for the middle and top column and 120, 160, 200, 240, 280, 300 min for the bottom column. Sample locations included the underdrain, D-25, and D-05. The D-25 and D-05 locations were chosen to collect samples from both mobile and immobile zones determined from previous tracer studies (Donaghue et al., 2022). To account for potential transitional effects between events, sample collection was omitted for Trans-2.5HLR-I and Trans-5HLR-I. A final pulse tracer test was performed at the end of transient events and confirmed flow patterns were not altered (Table S5, Fig. S1).

3. Results and discussion

3.1. Steady state NO_x removal, isotopes enrichment for mobile zones, and IWS non-ideal flow

NO_x removal efficiency (equation 5) increased as underdrain height decreased for all steady state events (Fig. 2). As HLR decreased from 5 to 1 cm/h, effluent NO_x removal increased from 25 to 99% for the bottom underdrain, 22 to 84% for the middle underdrain, and 10 to 52% for the top underdrain (Fig. 2, p-value < 0.05 for SS-2.5HLR and SS-5HLR). Superior performance observed for the bottom underdrain is attributed to longer HRTs relative to the middle and top underdrains heights (Table 1). For example, mean tracer residence times equaled 5.0 h, 3.8 h, and 3.5 h for the bottom, middle, and top column, respectively for an applied HLR of 5 cm/h. Others demonstrated how longer HRT increases NO_3^- removal (Halaburka et al., 2017; He et al., 2018). Studies considering regression on DO, temperature, influent NO_3^- concentration, and HRT indicated HRT contributed most (93%) to NO_3^- removal (Martin et al., 2019).

Figure_2

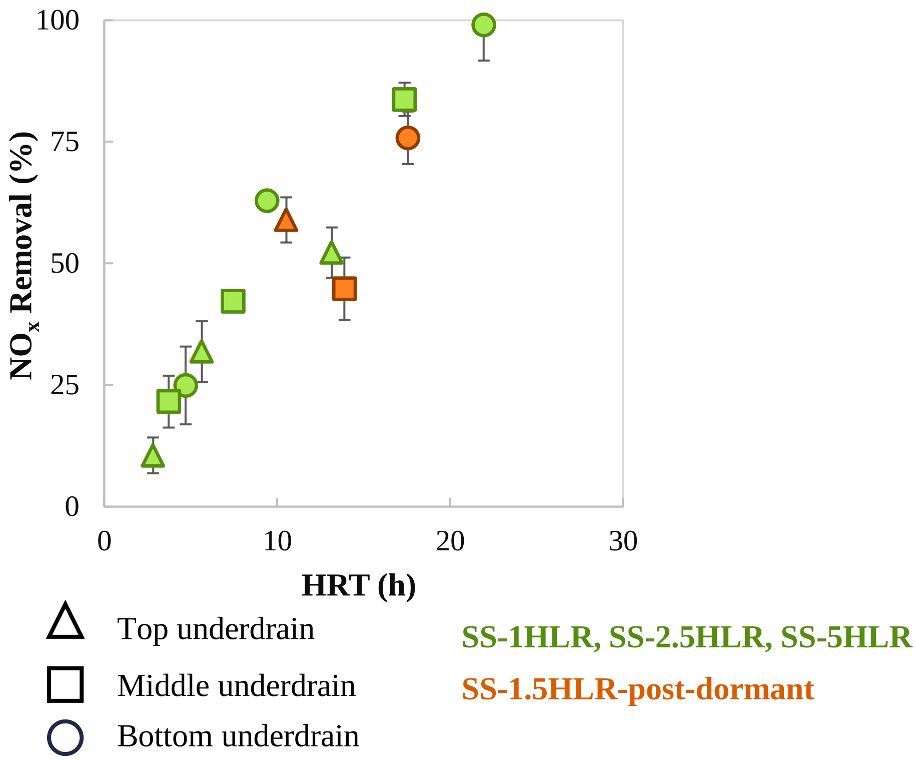

Fig 2

Percent NO_x removal observed at the underdrain as a function of hydraulic residence time (HRT). HRT was determined based on effective pore volume. r^2 values for events SS-1HLR, SS-2.5HLR, and SS-5 HLR equaled 0.9337.

The dual isotope data from SS-1HLR support the effectiveness of mobile zones in denitrification. The $\delta^{15}N$ versus $\delta^{18}O$ plot shows a 1:1 line indicating denitrification (Fig. 3a) with up to a 13‰ difference from the synthetic stormwater water. The middle and bottom columns showed a linear slope on the enrichment plots for both isotopes, which confirmed that denitrification was occurring (Fig. 3b). However, the top column showed a non-linear enrichment response, which indicated mixing of denitrified water and immobile zone water where NO_3^- mass transfer was limited. The isotope enrichment calculation helped distinguish between lower NO_3^- concentration due to mixing with immobile zone water and denitrification which removes NO_3^-. The enrichment factors of –5.2 and –4.7 for $\delta^{15}N$ versus $\delta^{18}O$ were close in value (Table 2) with slightly lower expected for $\delta^{18}O$. Isotope enrichment factors for middle and bottom underdrains were also similar although slightly lower for middle underdrain (-4.6 and –3.5 for $\delta^{15}N$ versus $\delta^{18}O$). Isotope enrichment for SS-1HLR versus SS-1.5HLR-post-dormant was also similar (-5.1 versus -5.4 for $\delta^{15}N$ and -4.5 versus -5.0 for $\delta^{18}O$) although the highest fractionation was observed for a single sample in SS-1HLR from the bottom underdrain.

Water quality parameters of DO, DOC, and NH_4^+ confirmed favorable conditions for denitrification existed in the IWS for all columns. Denitrification conditions require DO less than 3 mg-O_2/L (Gómez et al., 2002) and an adequate carbon source such as DOC leaching from woodchips (Newcomer et al., 2012). Steady state IWS DO concentrations (measured at 15 cm height) remained less than 0.2 mg-O_2/L across all three columns (Fig. S2a-S2b). Average DOC concentrations were 2.1 to 4.8 mg-C/L during SS-5HLR and decreased to non-detect levels (< 2 mg-C/L) during SS-2.5HLR. Decreasing DOC concentrations as HLR decreased is likely associated with longer HRT for NO_3^- removal and DOC utilization (Lynn et al., 2015a). During steady state, effluent NH_4^+ concentrations ranged from non-detect (i.e., ≤ 0.016 mg-N/L) to

Table 2. Enrichment factors calculated for steady state events.

Event	**^{15}N enrichment (Ɛ)**	**^{18}O enrichment (Ɛ)**	**Number of points**
All	-5.2	-4.7	8
SS-1HLR	-5.1	-4.5	3
SS-1.5HLR	-5.4	-5.0	5
Bottom - (SS-1HLR & SS-1.5HLR)	-5.4	-5.2	4
Middle - (SS-1HLR and SS-1.5HLR)	-4.6	-3.5	4

Figure_3

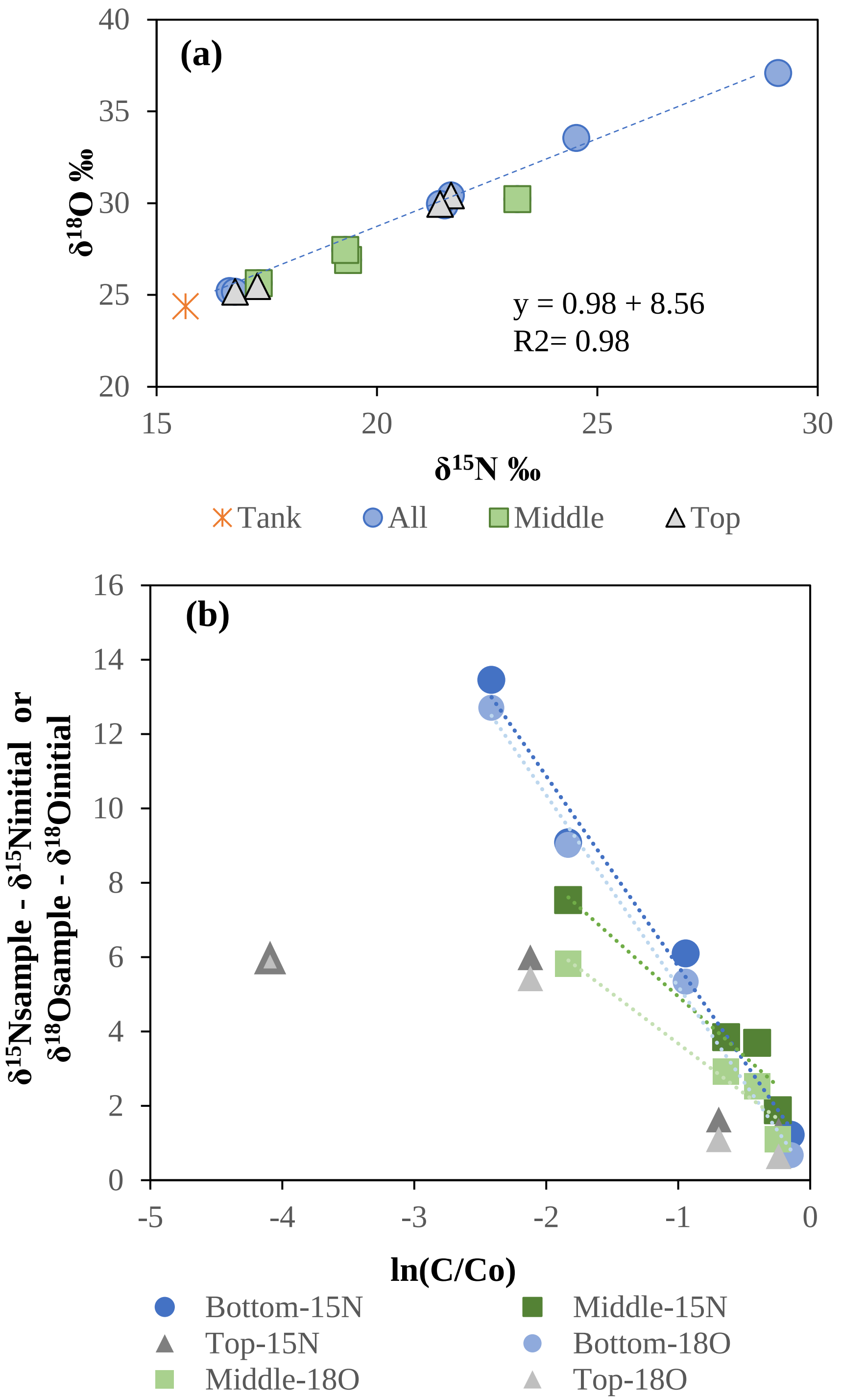

Fig 3

Steady state isotope data (a) dual isotope plot and (b) isotope enrichment plot. $\delta^{15}N$ and $\delta^{18}O$ plot along a denitrification line. Enrichment plot shows bottom and middle column plot along a line, but top column data do not, indicating low concentrations reflected the immobile zone rather than just denitrification.

0.156 mg-N/L (or < 4% of the TN concentration) and confirmed DNRA was not a primary pathway for NO_x removal. Average effluent pH (across all SS events) increased relative to synthetic stormwater (7.06 ± 0.03) to 7.36 ± 0.07, 7.34 ± 0.02, and 7.47 ± 0.09 for the bottom, middle, and top underdrain, respectively.

HLR affected *in situ* IWS NO_x concentration profiles as a function of depth (Fig. 4); however, transport across all three columns varied due to the presence and size of immobile zones. *In situ* two dimensional IWS sampling proved a useful approach to identify where processes occur and improve system design. For the bottom column, NO_x concentrations decreased as IWS sample port height decreased (i.e., approached the base). For SS-2.5HLR, average proximal IWS NO_x concentrations decreased from 2.9 to 1.6 mg-N/L as sample port height decreased from P-25 to P-05 cm (Fig. 4a). Additionally, the concentration difference between the P-25 to P-05 IWS sample height (i.e., NO_x(P-25) – NO_x(P-05)) increased from 0.50 to 2.2 mg-N/L as HLR decreased from 5 to 1 cm/h (Fig. 4a). The increased differential is attributed to increased residence time and consequently NO_x removal where denitrification was occurring.

IWS NO_x concentrations decreased substantially for regions below the middle and top underdrain heights and is likely attributed to limited mass transport into the immobile zones. For example, NO_x concentrations remained less than 0.04 mg-N/L for IWS locations P-20 through P-05 for the top column for SS-5HLR through SS-1HLR (Fig. 4c). Steady state bioretention column NO_x concentration profiles and dual isotope analysis coupled with tracer studies and flow modeling from previous work, suggest that while favorable conditions for denitrification exists in regions below the top and middle underdrain heights, NO_3^- removal is less efficient due to limited mass transport (i.e., limited NO_3^- exchange into the immobile zones)(Donaghue et al.,

Figure_4

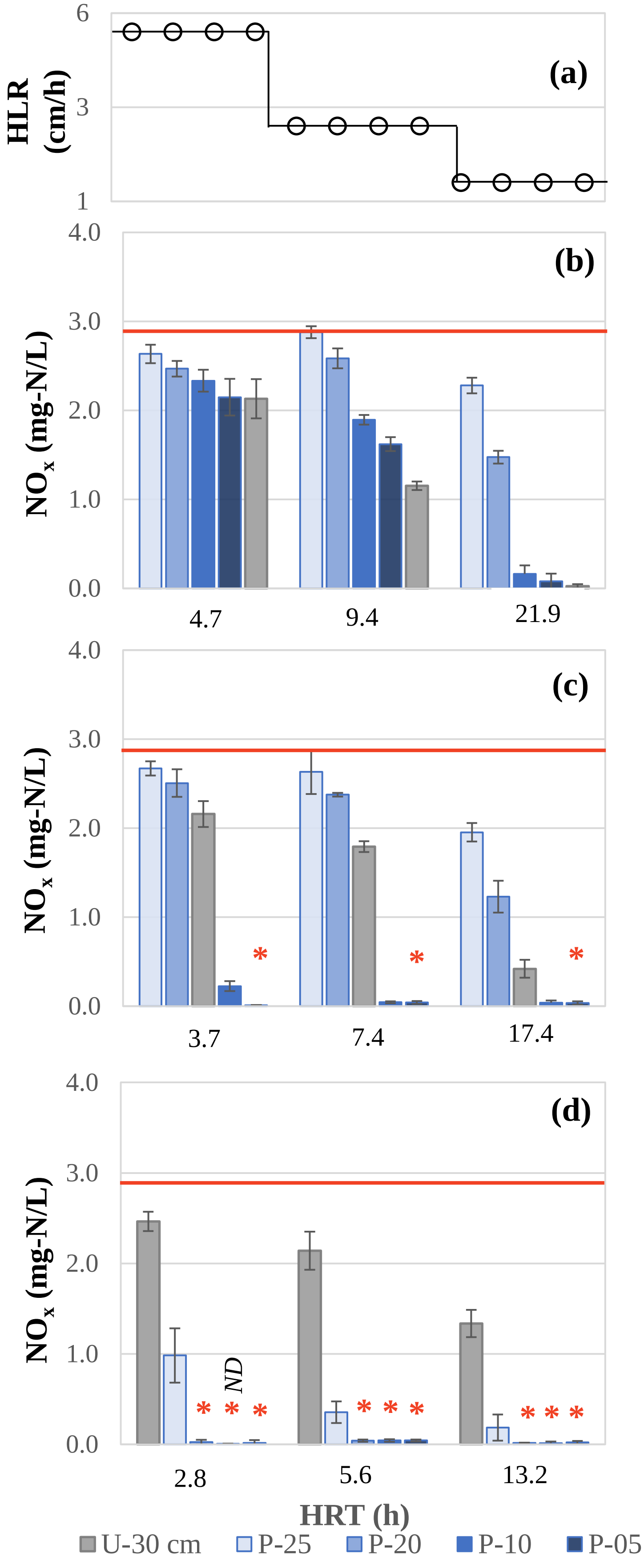

Fig 4

Steady state NO_x concentration profiles as a function of IWS underdrain height and (a) hydraulic loading rate (HLR) for (b) bottom (c) middle, and (d) top columns. Error bars equal to ± σ. Red asterisks (*) denotes immobile zones. Hydraulic residence time (HRT) is based of effective PVs. ND = non-detect (0.008 mg-N/L). The solid red line notes the average tank concentration (2.9 ± 0.26 mg-N/L).

2022). However, the degree of mass transport to the immobile zone is governed by the concentration gradient. Thus, higher influent NO_3^- concentrations would potentially increase mass transfer rates into this zone.

Velocity heat maps for the SS-1HLR (Fig. S3) illustrate the presence of immobile, or low flow, zones below the middle and top underdrain. Column tracer experiments and VS2DRTI flow and transport modeling conducted by this research group (Donaghue et al., 2022) for the same experimental design demonstrated the presence of immobile zones below the top underdrain (thickness ≤ 20 cm) and middle underdrain (thickness ≤ 5 cm). Calculated hydraulic efficiencies (e_v), the mean tracer residence time divided by the theoretical residence time, and tracer breakthrough curve statistics supported the presence of immobile zones. Specifically, e_v decreased from 1.0 to 0.76 as underdrain height increased from 1 to 30 cm. Hydraulic efficiencies < 1 indicate non-ideal flow where the mean tracer residence time is less than the theoretical residence time—an undesirable design scenario where treatment volume is underutilized. The presence of immobile zones suggests nonequilibrium flow where fluid is partitioned into regions of mobile (flowing) and immobile (stagnant) zones. Nonequilibrium flow includes a mass transfer coefficient as a third parameter to account for exchange between mobile and immobile zones (Field and Pinsky, 2000).

The effect of IWS underdrain configuration on system hydraulics and transport processes will also be influenced by the IWS width to depth ratio. The presence of immobile zones below the middle and top underdrain was specific to a case where the IWS width to depth ratio equaled 0.5 (15 cm width/30 cm depth). Two-dimensional flow patterns were observed in mobile regions of the IWS (Fig. S3) with higher velocity zones closest to the underdrain location. As a result, distal sample ports had longer residence times and demonstrated lower NO_3^- concentration profiles (Fig. S4). Simulations performed by our research group elsewhere (Donaghue et al., 2022) also considered IWS width to depth ratios greater than 1 (50 cm width/30 cm depth). For this scenario hydraulics efficiencies ranged 0.89 to 0.96 and immobile zones comprised less than 2% of the IWS. For IWS width to depth ratios greater than 1, velocity heat maps showed a wider distribution of velocities. While simulations indicated immobile zones were minimal for a IWS width to depth ratio of 1.67, maximizing HRT will still be an important factor for achieving higher NO_3^- removal efficiency.

3.2. Zero-order kinetics and evidence of IWS aging

Underdrain NO_x removal demonstrated a linear correlation with HRT (Fig. 2). For events SS-5HLR through SS-1HLR, higher correlations were observed for zero-order (k_0 = 3.21 g-N*m^{-3}*d^{-1}, r^2 = 0.946, Fig. S5a) compared to first-order kinetic estimates (k_1 = 4.25 d^{-1}, r^2 = 0.790, Fig. S5b). The rate model employed by Peterson et al. 2015 was used to determine rate constants (details in SI). Often, NO_3^- removal kinetics are considered zero-order where the reaction rate is controlled by an independent parameter (i.e., HRT or release of DOC from woodchips) rather than NO_3^-. Halaburka et al. observed zero-order kinetics for “aged” (saturated > 13 months) woodchip bioreactor columns for an input NO_3^- concentration of 10 mg-N/L and constant temperature (2017). First-order removal rates have been reported for laboratory bioreactor columns (influent of 1 to 6 mg-N/L)(Igielski et al., 2019). Additionally, transition to first-order kinetics may occur at lower NO_3^- concentrations (<0.5 mg-N/L)(Schipper et al., 2010). Addy et al. compiled data across 26 peer reviewed papers which included 14 bed field studies and 10 laboratory column woodchip bioreactor studies (2016). Authors reported that NO_3^- removal rates during the first year were more than 3 times higher than aged systems. Therefore, rates after year one of operation are more representative of performance long-term. Interestingly, columns in this current paper operated 5 months and did not meet the definition of "aged". Yet, observed zero-order rates agree with mean NO_3^- removal rates (2.8 $g\text{-}N*m^{-3}*d^{-1}$) for "aged" (13 to 24 month) bioreactors rather than younger (< 13-month-old) bioreactors (9.1 $g\text{-}N*m^{-3}*d^{-1}$) (Addy et al., 2016).

During SS-1.5HLR-postdormant (orange symbology, Fig. 2), removal rates for the middle and bottom underdrain decreased by 46% and 23%, respectively. These decreases are relative to the pre-dormant performance and the percent removal deviated from linear trends observed during SS-5HLR through SS-1HLR (green symbology). NO_3^- removal rates can vary during the initial one to three years of operation before stabilizing (Addy et al., 2016). One column study using wood pulp and sand media reported a 50% decline in NO_3^- removal efficiency within 1 year of operation (Robertson et al., 2008). Higher NO_3^- removal rates that occurred during early operation were attributed to woodchips leaching excess organic material, but leaching rates stabilized after extended use (Halaburka et al., 2017). For bioretention systems, IWS media may not remain permanently saturated between precipitation events due to evapotranspiration and exfiltration to underlying media. The 4.5-month dormant period during COVID here represented an exaggerated ADP case. However, the observed decline in NO_3^- removal for the bottom and middle underdrains suggest prolonged exposure to semi-saturated conditions could contribute to woodchip aging. As stated above, the isotope data showed the largest fractionation for a single sample in SS-1HLR, but similar enrichment factors before and after the 4.5-month dormant period (Table 2).

3.3. NO_x, dual isotope, and water quality patterns for transient events under different HLR

As transient event HLR increased, a higher fraction of old IWS water was replaced with new incoming synthetic stormwater. Consequently, NO_x concentrations (Fig. 5b) and the mass

Figure_5

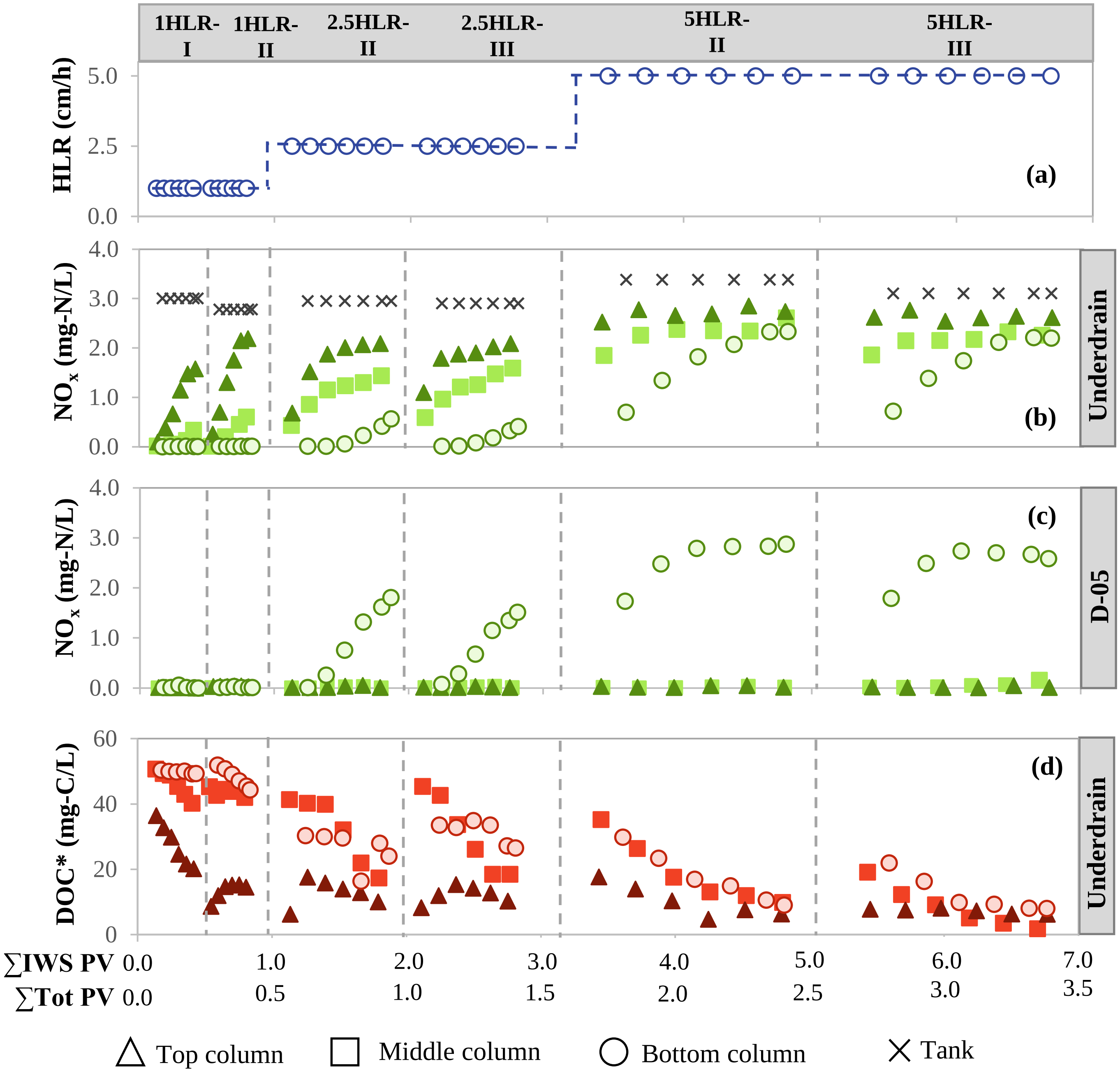

Fig 5
Water quality results for transient events withs variable hydraulic loading rate (HLR). Prior to transient events, a total of ~150 total PVs were applied to each column across steady state conditions and tracer tests. *absorbance measured at 254 nm.

flux of NO_x leaving the system (Table S7) increased at the underdrain for all three columns. In between transient flow, water was stored in the IWS for a prolonged residence time (7 days) (Trans-1HLR-I through Trans-5HLR-III) and is more relevant to field conditions. The bottom column performed best in minimizing the mass flux of NO_x from the underdrain followed by the middle and the top columns (Fig. 5b, Table S7). For the highest HLR (5 cm/h) tested during transient events, the applied IWS pore volume was 2.3 (total pore volume equaled 1); the final C/C_o ranged from 0.69 to 0.84 (Fig. 5b, Fig. S6) and suggested NO_3^- removal. Furthermore, final C/C_o for Trans-5HLR was similar to NO_3^- removal efficiency (=100%*(1-C/C_o)) observed during steady state, SS-5HLR, which ranged from 10 to 25% (C/C_o = 0.75 to 0.90).

NO_x concentration profiles for the D-05 location highlighted the underutilization of treatment volume for a portion of the IWS below the middle and top columns during events (Fig. 5c). For Trans-2.5HLR and Trans-5HLR, the bottom column NO_x concentration profiles for the underdrain and D-05 followed similar breakthrough patterns (Fig. 5c). Average normalized peak NO_x concentrations for the bottom column D-05 location equaled 0.57 and 0.84 mg-N/L for Trans-2.5HLR and Trans-5HLR, respectively. In contrast, the middle and top column, normalized C_{peak} NO_x concentrations at the D-05 location remained 97% less than the influent concentration across all HLR events (Fig. 5c). Low NO_x concentrations observed at D-05 for the middle and top column are likely attributed to presence of an immobile zone and limited mass transport below raised underdrains (Donaghue et al., 2022). However, the IWS volume below raised underdrains was not entirely characterized by an immobilize zone. Top column IWS NO_x concentration profiles at the conclusion of Trans-2.5HLR-II and III demonstrated that mixing and mass transport occurred a certain depth below the underdrain (Fig. 6a). For example, D-25

NO_x was ~2.2 mg-N/L but ranged from non-detect to 0.16 mg-N/L for location D-05 to D-20 (Fig. 6a).

Old IWS water (t = 0 min) NO_x concentrations were considerably lower relative to the final event concentrations (t = 300 min) (Fig. 6). This cycle is observed over multiple events (Fig. 5) and suggested that NO_x removal also occurred between storms. For example, at the conclusion of Trans-2.5HLR-I (t=300 min sample time) the bottom column IWS NO_x concentrations were 2.9 mg-N/L (D-25) and 1.8 mg-N/L (D-05) (Fig. 6a, Table S8). In contrast corresponding old IWS water NO_x concentrations declined more than 94% and equaled 0.17 mg-N/L (D-25) and 0.04 mg-N/L (D-05) (Fig. 6b).

All three columns showed a linear slope between $\delta^{15}N$ and $\delta^{18}O$ (Fig. 7a) and isotope enrichment factors indicated denitrification (Table 3) albeit with limited data for the top column due to little change in NO_3^- concentrations. Trans-1HLR and Trans-2.5HLR showed roughly half the enrichment of steady state (-2.7 to -3.8 for $\delta^{15}N$ and -1.6 to -2.9 for $\delta^{18}O$), while Trans-5HLR showed higher enrichment (-7.6 to –9.6 for $\delta^{15}N$ and –5.1 to –6.5 for $\delta^{18}O$). However, there were limited data for the middle and top columns for Trans-5HLR; additionally, some points did not fall on a linear enrichment trend (e.g., the bottom underdrain at t = 180 min; Fig. S7). Where sufficient data were available, the slopes (enrichment factors) for t = 180 min and t = 300 min were similar, excluding the outliers (Fig. 7b,c). In some cases (Trans-1HLR and top column Trans-2.5HLR) the $\delta^{18}O$ data were not linear, unlike the steady state conditions. The higher enrichment for Trans-5HLR may be a reflection of more NO_3^- mass that was applied and available for processing at the higher flow. For example, ~50 mg-N were applied for Trans-5HLR compared to ~10 mg-N applied during Trans-1HLR.

Table 3. Enrichment factors calculated for transient events. Points that did not fall on a linear trend were excluded from the slope calculation as indicated under the Dataset column. For the bottom column intermediate time is 200 minutes, and for the middle and top columns it is 180 minutes. Orange shading indicates insufficient data.

Event	**Dataset**	**^{15}N enrichment (Ɛ)**	**^{18}O enrichment (Ɛ)**	**Number of points**
Trans-1.5HLR	all	-2.7	-1.6	8
Trans-2.5HLR	all but bottom column T200min	-3.8	-2.9	12
Trans-5HLR	all but bottom column D-05 and D-25, T200min	-7.6	-5.1	6
Trans-1HLR	all	-2.7	-1.6	8
Trans-1HLR	bottom column	-2.9		2 δ^{18}O not linear
Trans-1HLR	middle column	-2.7	-1.8	2
Trans-1HLR	top column	-2.7	-1.8	4
Trans-2.5HLR	all but bottom underdrain T200min	-3.8	-2.9	12
Trans-2.5HLR	bottom column	-3.7	-3.0	3
Trans-2.5HLR	middle column	-3.0	-1.8	4 (2 off scale)
Trans-2.5HLR	top column			4 (not linear)
Trans-5HLR	all but bottom column D-05, D-25 T200 min	-7.6	-5.1	6
Trans-5HLR bottom c.	bottom column	-7.5	-5.1	4
Trans-5HLR	middle column			1 insufficient data
Trans-5HLR	top column			1 insufficient data
Trans-1HLR	all	-2.7	-1.6	8
Trans-1HLR	T300 min	-2.9	-2.0	4
Trans-1HLR	T180-200 min	-2.6		4 δ^{18}O not linear
Trans-2.5HLR	all but bottom underdrain T200 min	-3.8	-2.9	12
Trans-2.5HLR	T300 min	-3.8	-3.0	6
Trans-2.5HLR	T180-200 min	-3.8	-2.8	6
Tanns-5HLR	all but bottom column D-05, D-25 T200 min	-7.6	-5.1	6
Trans-5HLR	T300 min	-9.6	-6.5	5
Trans-5HLR	T180-200 min			1 insufficient data

Figure_6

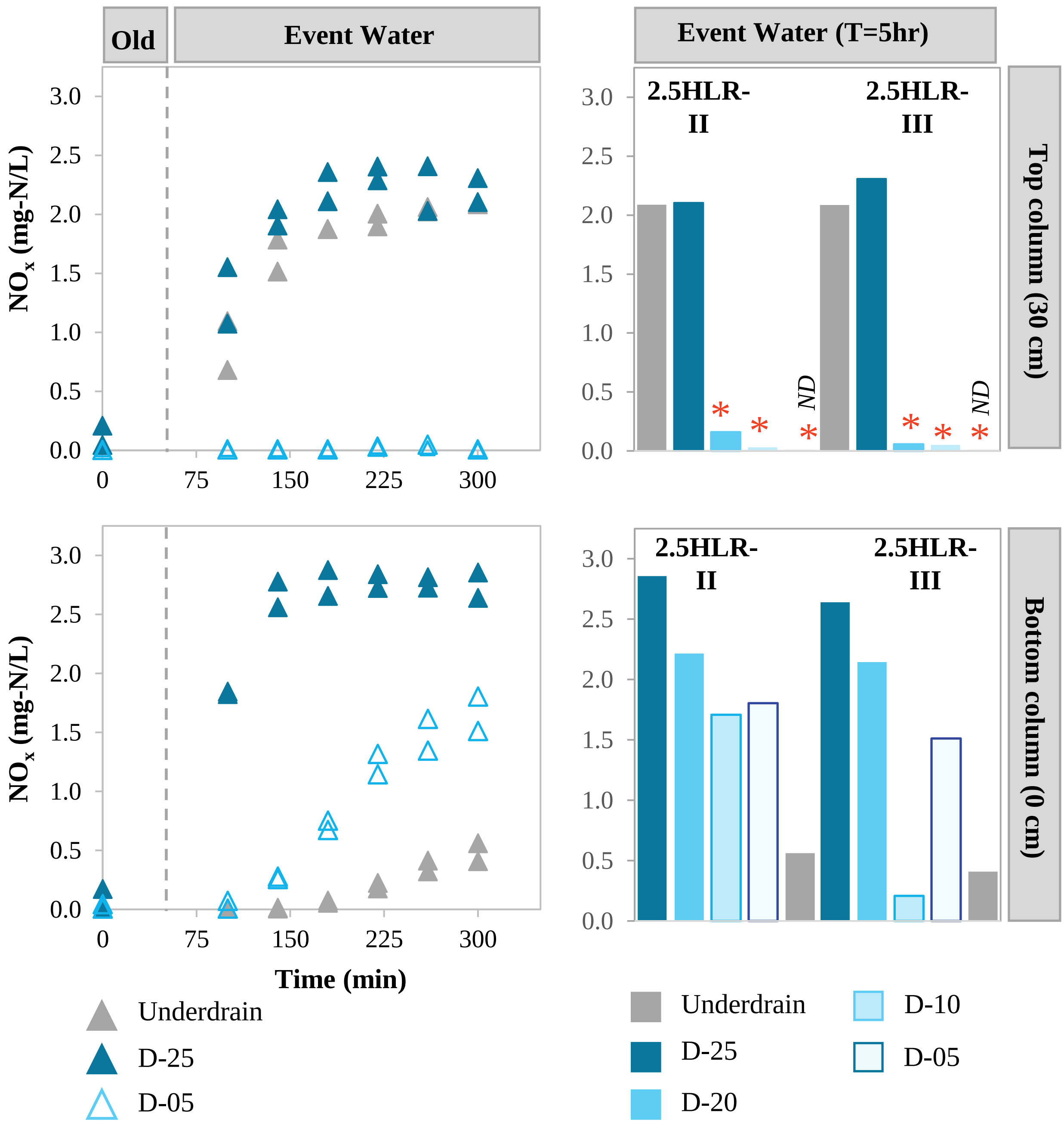

Fig 6

Comparison NO_x concentration profiles for top and bottom columns for Trans-2.5HLR event. *denotes immobile zones. ND = non-detect (0.008 mg-N/L). Event water includes mixture of old IWS water and new synthetic stormwater.

Figure_7

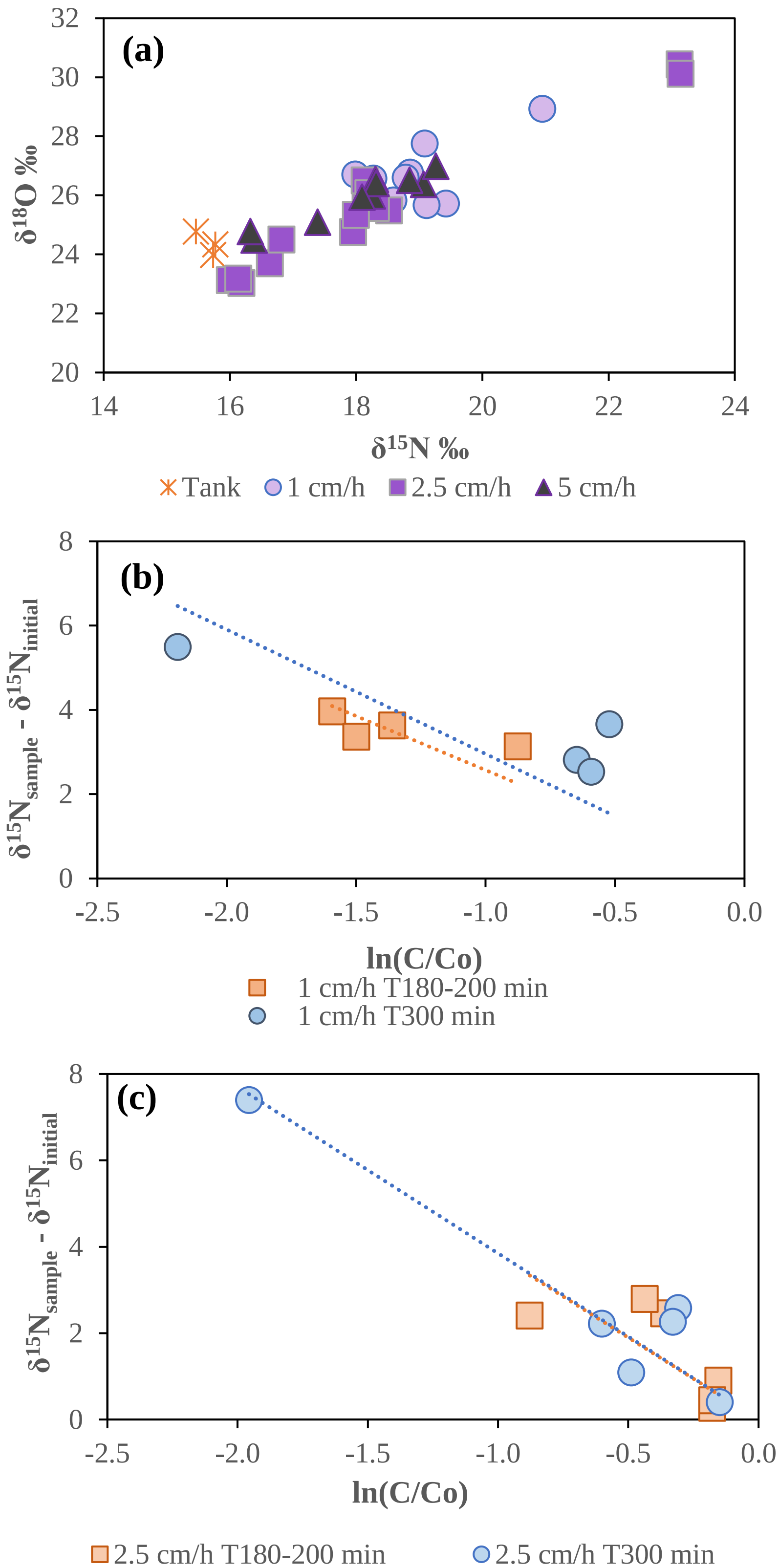

Fig 7
Transient isotope data for (a) dual isotope plot and isotope enrichment plots for (b) Trans-1HLR and (c) Trans-2.5HLR events. Insufficient data to compare time steps for Trans-5HLR events. $\delta^{15}N$ and $\delta^{18}O$ plot along a denitrification line for all three HLR. Enrichment plot shows similar slopes for time steps (T) of 180-200 min and 300 min samples. For the bottom column intermediate time is 200 minutes, and for the middle and top columns it is 180 minutes.

During transient flow, effluent pH was less than synthetic stormwater (~7.0) and effluent peak DOC concentrations were associated with old IWS water and occurred at the beginning of events. Hydrolysis of woodchips produces volatile fatty acids and is associated with a decrease in pH (Lynn et al., 2015a). Except for event Trans-1HLR-I, average effluent pH was 6.7 (bottom underdrain) and 6.6 (middle and top underdrains) (Table S9). Other woodchip bioreactor columns demonstrated decreased pH relative to influent conditions under transient flow (Lynn et al., 2015a; Peterson et al., 2015). During dry periods, fungi and bacteria can degrade lignocellulose biomass like woodchips which increases DOC concentrations in porewater (Lynn et al., 2015b; Malherbe and Cloete, 2002). Concomitant with decreased pH, effluent DOC concentrations spiked at the beginning of event sampling (first ~0.1 to 0.25 total PVs) except for the top underdrain (Fig. 5d). Compared to steady state conditions, transient IWS water quality highlights the role dry periods play in promoting DOC leaching for potential denitrification. DON was observed in effluent across all three columns (Fig. S8a) and NH_4^+ was non-detect for most events (Fig. S8b) (see discussion in SI).

Generally, the top column resulted in lower effluent DOC mass flux (Table S7, Fig. S9 and DOC concentrations (Fig. 5d) from the underdrain. This is attributed to more mixing between old IWS water and new water during events compared to the bottom column. For the Trans-5HLR scenario, NO_x and DOC mass flux released from the bottom underdrain were 298 mg-N/m^2 and 3,560 mg-C/m^2, respectively compared to 564 mg-N/m^2 and 1980 mg-C/m^2 for the top underdrain (Table S7). For the middle underdrain, NO_x and DOC mass fluxes were 449 mg-N/m^2 and 3,360 mg-C/m^2 for Trans-5HLR scenarios. Opposing trends observed between effluent DOC and NO_x mass fluxes highlight two important considerations regarding underdrain placement. First, under transient conditions, raised underdrains promote mixing between old

IWS water and new water relative to the bottom column and provide an opportunity to utilize DOC built up during ADPs for denitrification. For the top column, old IWS water DOC concentrations ranged from 3.8 to 26 mg-C/L for P-25 and ranged from 30 to 36 mg-C/L for P-05 (Fig. S10a). In contrast, old IWS water DOC concentrations for the bottom column were consistent across the P-25 and P-05 locations (Fig. S10a). Following application of new stormwater two trends occurred for the top column: 1) P-05 IWS DOC concentrations spiked and 2) the final event concentration gradient between the P-25 and P-05 increased with increasing HLR. For example, the gradient ranged from 0.41 to 0.76 mg-C/L/cm for Trans-1HLR and ranged from 2.2 to 2.7 mg-C/L/cm for Trans-5HLR (Fig. S10a). During transient flow for the top column, incoming new stormwater pushed a fraction of old IWS water, with increased DOC, to the P-05 location. This transport phenomena was supported by transient chloride tracer storms conducted previously where chloride (a conservative tracer) accumulated at the P-05 location over the course of four transient events (Fig. S4 in Donaghue et al., 2022). However, DOC concentrations in old IWS water declined before the next event suggesting utilization (Fig. S10a-c) and likely higher DOC mass transfer rates to immobile regions during flow conditions. A second consideration for underdrain placement is that for bioretention systems, release of labile DOC to receiving water bodies is also an undesirable outcome and could potentially increase the biological oxygen demand.

Column studies with a bottom underdrain IWS commonly assume ideal plug flow when describing NO_3^- removal (Igielski et al., 2019; Lynn et al., 2017; Subramaniam et al., 2016) and immobile zones are assumed absent or minimal. However, flow conditions were classified as non-ideal for the middle and top columns as demonstrated by hydraulic efficiencies ≤ 1 (Donaghue et al., 2022). The extent of the immobile zone is also impacted by the HLR; we previously demonstrated that the immobile zone fraction decreased from 36 to 14% as HLR increased from 4 to 13 cm/h (Donaghue et al., 2022). Thus, site infiltration rates will also influence optimal underdrain height within the IWS in order to promote mixing with old IWS water and enhance NO_3^- removal during storm events.

3.4. Impact of ADP on NO_x and isotope patterns

For ADP conditions, the NO_x mass flux increased in the order of bottom column < middle column < top column and longer ADPs generally resulted in lower NO_x mass fluxes (Table S7) and concentrations from the bottom and middle columns. For example, the middle underdrain average NO_x mass flux was 69 mg-N/m^2 after 14 days compared to 106 mg-N/m^2 after 3 days (Table S7). Final normalized NO_x concentrations (C/C_o) for the middle underdrain decreased from 0.55 to 0.26 as ADP increased from 3 to 14 days. For the top underdrain, average NO_x mass flux decreased from 215 to 166 mg-N/m^2 as ADP increased from 3 to 7 days; the average mass NO_x flux was 188 mg-N/m^2 following 14 days. Unlike the middle underdrain, final normalized NO_x concentrations ranged 0.70 to 0.74 and did not show a decreasing trend as ADP increased from 3 to 14 days.

DOC concentrations in old IWS water generally did not increase as ADP increased from 3 to 14 days, with the exception of a few events. For example, P-05 old IWS water DOC concentrations ranged from 18.5 to 30.2 mg-C/L across the variable ADPs considered (Fig. S11a). But old IWS water DOC concentrations for the middle column P-05 increased from 16 to 31 mg-C/L between consecutive events Trans-7ADP-III and Trans-14ADP-II (Fig. S11b). Previous columns studies with similar IWS media composition reported increasing old IWS water DOC concentrations as ADP increased from 0 to 16 days (analytical methods differed) (Lynn et al., 2015a). Authors attributed concurrent DOC build up with increased dry periods to

DOC leaching rates exceeding DOC utilization rates. However, Lynn et al. observed that DOC leaching declined over longer ADP periods; the maximum DOC concentration of ~114 mg-C/L occurred following a 14 day ADP but decreased to ~ 76 mg-C/L after a 30 day ADP (2015a).

Isotope data collected to monitor ADP focused on evaluating the end of the dry period (labeled as t = 0 min associated with the subsequent transient event). The isotope data neither confirmed nor contradicted the ADP assessment because NO_3^- concentrations were low at the end of the dry periods. These low concentrations limited analytical precision for the isotope analysis. Only one sample submitted for analysis met the data quality requirements. The one sample with sufficient NO_3^- indicated a second source of NO_3^- released during the dry period with 2‰ lower $\delta^{15}N$ than the synthetic stormwater composition (likely woodchip organic matter). Five samples that were below the suggested detection limits also showed lower $\delta^{15}N$ than the synthetic stormwater. A possible scenario is that fractionation went to completion and the isotope signal for denitrification was "lost". This highlights an important consideration when incorporating isotope analysis and suggests isotope sample collection should target the time period immediately following the storm event (i.e., ~3-5 h post storm) rather than the end of the ADP.

3.5. IWS design considerations and environmental implications

IWS design for water quality and NO_3^- removal is relevant to nutrient sensitive watersheds where one point of regulation is storm sewer systems. Under these applications, maximizing HRT during a storm event is critical to enhance NO_3^- removal during a storm. For example, the underdrain could extend several feet from the outlet structure rather than span the entire length of the basin. This design would increase travel time. While not tested in this study, other design components in addition to IWS underdrain height can be included to enhance water quality. For example, an area of impermeable liner could be placed between overlying fill media and the IWS near the outlet location to prevent suspected short circuiting. Additionally, baffles could be implemented into the IWS to minimize immobile zones.

Operation and maintenance considerations may also influence IWS underdrain placement. Gas buildup from denitrification can cause impediments to flow and was observed to occur during ADPs of this study. Between storms, raised underdrains provide a release conduit, which may help maintain intended hydrology. We recognized in our previous work that issues with the underdrain clogging, due to sediment, are minimized when the underdrain is raised compared to bottom underdrain configurations (Donaghue et al., 2022).

In situ IWS sampling reveals spatial and temporal variations related to transport processes. Limiting sampling to inlet and outlet locations may overlook the presence and influence of immobile zones on system performance—a critical component to improving GSI design. Additionally, dual isotope analysis is a valuable tool to distinguish whether low NO_3^- concentrations are a result of denitrification or dilution during storm events. However, the application of dual isotope approaches is limited for studying dry periods if NO_3^- concentrations are below detection limits. Therefore, it is important to collect enough samples to follow temporal trends before dilution occurs. If additional NO_3^- sources occur during prolonged ADPs, dual isotopes can be used to identify them in field or laboratory systems.

4. Conclusions

Specific conclusions from this study include the following:

- NO_3^- removal efficiency increased with increasing HRT and zero-order kinetics were observed across all three IWS underdrain heights for steady state. As a result, IWS design strategies that increase HRT will enhance NO_3^- removal efficiency. For steady state conditions tested here, the bottom column always outperformed the middle and top columns with respect to NO_x removal because of longer residences times.

- Steady state NO_x removal decreased following a 4.5-month duration when the IWS was partially saturated. Woodchip longevity and effectiveness may become compromised in climates with extended dry periods or if the IWS water level lowers due to exfiltration between storms. Impermeable liners at the base of IWS could help to mitigate this challenge.
- Under steady state conditions, immobile zones, created by underdrains at the top of the IWS, reduced hydraulic efficiency and limited denitrification despite low DO and a sufficient carbon source. Contrasting NO_3^- isotope enrichment trends support this conclusion, where the mobile zone exhibited linear NO_3^- isotope enrichment response (for both isotopes) compared to non-linear NO_3^- isotope enrichment response for the top column.
- For transient events, a linear NO_3^- isotope enrichment response was observed across all columns regardless of IWS underdrain height. While effluent NO_x concentrations converged across all columns for the highest HLR, the top underdrain resulted in lower effluent DOC mass fluxes. These results suggests that during storm conditions, top underdrains enhance mixing between old IWS water and new stormwater which allows microbes to utilize DOC built up during ADPs and enhance denitrification during storm events.
- An IWS underdrain configured at the bottom of the IWS increased residence time but can force plug flow conditions that limit mixing with old IWS water and utilization of DOC.

IWS design for water quality enhancement will require incorporating measures that balance denitrification with DOC exportation. Design decisions may include an underdrain located mid depth of the IWS to promote mixing, shortening the length of the underdrain to minimize short circuiting, or incorporating impermeable liners at discrete locations between fill media and the IWS to increase travel times.

Acknowledgements

This work was supported by the Pennsylvania Sea Grant under Grant No. S000160-NOAA.

Authors would like to thank Willow Neske for support with column sampling collection.

Appendix A. Supplementary material

Supplementary material to this article can be found on the online version.

References

Abusallout, I., Hua, G., 2017. Characterization of dissolved organic carbon leached from a woodchip bioreactor. Chemosphere 183, 36–43. https://doi.org/10.1016/j.chemosphere.2017.05.066

Addy, K., Gold, A.J., Christianson, L.E., David, M.B., Schipper, L.A., Ratigan, N.A., 2016. Denitrifying Bioreactors for Nitrate Removal: A Meta-Analysis. J. Environ. Qual. 45, 873–881. https://doi.org/10.2134/jeq2015.07.0399

Berger, A.W., Valenca, R., Miao, Y., Ravi, S., Mahendra, S., Mohanty, S.K., 2019. Biochar increases nitrate removal capacity of woodchip biofilters during high-intensity rainfall. Water Res. 165, 115008. https://doi.org/10.1016/j.watres.2019.115008

Brown, R., Hunt, W., Kennedy, S., 2009. Urban Waterways: Designing Bioretention with an Internal Water Storage (IWS) Layer. North Carolina Coop. Ext. Serv. 1–14.

Bu, C., Wang, Y., Ge, C., Ahmad, H.A., Gao, B., Ni, S., 2017. Dissimilatory Nitrate Reduction to Ammonium in the Yellow River Estuary: Rates, Abundance, and Community Diversity. Sci. Rep. 1–11. https://doi.org/10.1038/s41598-017-06404-8

Burgis, C.R., Hayes, G.M., Zhang, W., Henderson, D.A., Macko, S.A., Smith, J.A., 2020. Tracking denitrification in green stormwater infrastructure with dual nitrate stable isotopes. Sci. Total Environ. 747, 1–11.

Burns, D.A., Boyer, E.W., Elliott, E.M., Kendall, C., 2009. Sources and Transformations of Nitrate from Streams Draining Varying Land Uses: Evidence from Dual Isotope Analysis. J.

Environ. Qual. 38, 1149–1160. https://doi.org/10.2134/jeq2008.0371

Carey, R.O., Hochmuth, G.J., Martinez, C.J., Boyer, T.H., Dukes, M.D., Toor, G.S., Cisar, J.L., 2013. Evaluating nutrient impacts in urban watersheds: Challenges and research opportunities. Environ. Pollut. 173, 138–149. https://doi.org/10.1016/j.envpol.2012.10.004

Currie, W., 2007. Modeling the dynamics of stable-isotope ratios for ecosystem biogeochemistry. In Stable Isotopes in Ecology and Environmental Science, 2nd ed. Blackwell Publishing, London.

Donaghue, A.G., Beganskas, S., McKenzie, E.R., 2022. Inverted versus Raised: The Impact of Bioretention Underdrain Height on Internal Water-Storage Hydraulics. J. Sustain. Water Built Environ. 8, 1–12. https://doi.org/10.1061/jswbay.0000974

Ebina, J., Tsutsui, T., Shirai, T., 1983. Simultaneous determination of total nitrogen and total phosphorus in water using peroxodisulfate oxidation. Water Res. 17, 1721–1726. https://doi.org/10.1016/0043-1354(83)90192-6

Field, M.S., Pinsky, P.F., 2000. A two-region nonequilibrium model for solute transport in solution conduits in karstic aquifers. J. Contam. Hydrol. 44, 329–351. https://doi.org/10.1016/S0169-7722(00)00099-1

Gómez, M.A., Hontoria, E., González-López, J., 2002. Effect of dissolved oxygen concentration on nitrate removal from groundwater using a denitrifying submerged filter. J. Hazard. Mater. https://doi.org/10.1016/S0304-3894(01)00353-3

Halaburka, B.J., Lefevre, G.H., Luthy, R.G., 2017. Evaluation of Mechanistic Models for Nitrate Removal in Woodchip Bioreactors. Environ. Sci. Technol. 51, 5156–5164. https://doi.org/10.1021/acs.est.7b01025

He, S., Ding, L., Pan, Y., Hu, H., Ye, L., Ren, H., 2018. Effect of hydraulic retention time on nitrogen removal and functional gene quantity/transcription in biochar packed reactors at 5 °C: A control-strategy study. Bioresour. Technol. 264, 400–405. https://doi.org/10.1016/j.biortech.2018.06.006

Igielski, S., Kjellerup, B. V., Davis, A.P., 2019. Understanding urban stormwater denitrification in bioretention internal water storage zones. Water Environ. Res. 91, 32–44. https://doi.org/10.2175/106143017x15131012188024

Kendall, C., Elliott, E.M., Wankel, S.D., 2007. Tracing Anthropogenic Inputs of Nitrogen to Ecosystems. Stable Isot. Ecol. Environ. Sci. Second Ed. 375–449. https://doi.org/10.1002/9780470691854.ch12

Kim, H., Seagren, E.A., Davis, A.P., Kim, H., Seagren, E.A., Davis, A.P., 2003. Engineered Bioretention for Removal of Nitrate from Stormwater Runoff. Water Environ. Res. 75, 355–367.

Li, L., Yang, J., Davis, A.P., Liu, Y., 2019. Dissolved Inorganic Nitrogen Behavior and Fate in Bioretention Systems: Role of Vegetation and Saturated Zones. J. Environ. Eng. 145, 04019074. https://doi.org/10.1061/(asce)ee.1943-7870.0001587

Lynn, T., Yeh, D., Ergas, S., 2015a. Performance of Denitrifying Stormwater Biofilters Under Intermittent Conditions. Environ. Eng. Sci. 32, 796–805. https://doi.org/10.1089/ees.2015.0135

Lynn, T., Yeh, D., Ergas, S., 2015b. Performance and Longevity of Denitrifying Wood-Chip Biofilters for Stormwater Treatment: A Microcosm Study. Environ. Eng. Sci. 32, 321–330. https://doi.org/10.1089/ees.2014.0358

Lynn, T.J., Nachabe, M.H., Ergas, S.J., 2017. Modeling Denitrifying Stormwater Biofilters Using SWMM5. J. Environ. Eng. (United States) 143, 1–10. https://doi.org/10.1061/(ASCE)EE.1943-7870.0001209

Malherbe, S., Cloete, T.E., 2002. Lignocellulose biodegradation: Fundamentals and applications. Environ. Sci. Biotechnol. 1.

Mariotti, A., Germon, J.C., Hubert, P., Kaiser, P., Letolle, R., Tardieux, A., Tardieux, P., 1981. Experimental determination of nitrogen kinetic isotope fractionation: Some principles; illustration for the denitrification and nitrification processes. Plant Soil 62, 413–430. https://doi.org/10.1007/BF02374138

Martin, E.A., Davis, M.P., Moorman, T.B., Isenhart, T.M., Soupir, M.L., 2019. Impact of hydraulic residence time on nitrate removal in pilot-scale woodchip bioreactors. J. Environ. Manage. 237, 424–432. https://doi.org/10.1016/j.jenvman.2019.01.025

Moorman, T.B., Parkin, T.B., Kaspar, T.C., Jaynes, D.B., 2010. Denitrification activity, wood loss , and N2O emissions over 9 years from a wood chip bioreactor. Ecol. Eng. 36, 1567–1574. https://doi.org/10.1016/j.ecoleng.2010.03.012

Newcomer, T.A., Kaushal, S.S., Mayer, P.M., Shields, A.R., Canuel, E.A., Groffman, P.M., Gold, A.J., 2012. Influence of natural and novel organic carbon sources on denitrification in forest, degraded urban, and restored streams. Ecol. Monogr. https://doi.org/10.1890/12-0458.1

Peterson, I.J., Igielski, S., Davis, A.P., Asce, F., 2015. Enhanced Denitrification in Bioretention Using Woodchips as an Organic Carbon Source 1, 1–9. https://doi.org/10.1061/JSWBAY.0000800.

Robertson, W.D., Vogan, J.L., Lombardo, P.S., 2008. Nitrate Removal Rates in a 15-Year-Old Permeable Reactive Barrier Treating Septic System Nitrate 65–72.

Schipper, L.A., Robertson, W.D., Gold, A.J., Jaynes, D.B., Cameron, S.C., 2010. Denitrifying bioreactors — An approach for reducing nitrate loads to receiving waters. Ecol. Eng. 36, 1532–1543. https://doi.org/10.1016/j.ecoleng.2010.04.008

Sebilo, M., Aloisi, G., Mayer, B., Perrin, E., Vaury, V., Mothet, A., Laverman, A.M., 2019. Controls on the Isotopic Composition of Nitrite (δ15N and δ18O) during Denitrification in Freshwater Sediments. Sci. Rep. 9, 1–14. https://doi.org/10.1038/s41598-019-54014-3

Subramaniam, D., Ph, D., Mather, P., Russell, S., Rajapakse, J., Ph, D., 2016. Dynamics of Nitrate-Nitrogen Removal in Experimental Stormwater Biofilters under Intermittent Wetting and Drying 142, 1–12. https://doi.org/10.1061/(ASCE)EE.1943-7870.0001043.

United States Geological Survey (USGS), 2019. VS2DRTI.

Whitehead, P.G., Wilby, R.L., Battarbee, R.W., Kernan, M., Wade, A.J., 2009. A review of the potential impacts of climate change on surface water quality 6667. https://doi.org/10.1623/hysj.54.1.101

Yang, Y.Y., Toor, G.S., 2016. δ15N and δ18O Reveal the Sources of Nitrate-Nitrogen in Urban Residential Stormwater Runoff. Environ. Sci. Technol. 50, 2881–2889. https://doi.org/10.1021/acs.est.5b05353

Zhang, Y., Shi, P., Song, J., Li, Q., 2019. Application of nitrogen and oxygen isotopes for source and fate identification of nitrate pollution in surfacewater: A review. Appl. Sci. 9. https://doi.org/10.3390/app9010018